Monte Carlo simulation of jets in the upsilon and t-quarkonium regions

Cho-Kuen Ng
Department of Physics, University of Illinois at Urbana-Champaign, 1110 W. Green Street, Urbana, Illinois 61801
(Received 20 December 1985)

We apply Webber's QCD branching Monte Carlo model to study the properties of jets produced in upsilon decay and the nearby continuum e^+e^- annihilations. In general, agreement between the Monte Carlo simulation and data is obtained. More baryons are produced in upsilon decay than in the continuum annihilation because there are more heavy colorless clusters in the configuration of upsilon decay. We then investigate the various decay mechanisms of t-quarkonium. The heavy-particle spectra are found to be quite different for various decay modes of t-quarkonium.

I. INTRODUCTION

In recent years, much effort has been put into understanding the formation of jets in high-energy processes in the framework of quantum chromodynamics, especially in e^+e^- collisions, deep-inelastic scattering, and the Drell-Yan process. In order to account for the bulk properties of the particles coming out in the jets, a realistic description of jet evolution is necessary. Therefore, various Monte Carlo schemes have been proposed to simulate the evolution of jets in high-energy processes.[1,2]

As we all know, QCD has the properties of asymptotic freedom and confinement, and therefore it is convenient to divide high-energy processes into two different scales. At the high-energy scale, the processes can be well described by the QCD-improved parton model. The development of jets at the parton level is determined by perturbative QCD through the Altarelli-Parisi equations. At the low-energy scale, the strong coupling constant $\alpha_s(Q^2)$ increases and perturbative calculations become unreliable. In the real world, what we observe are hadrons, not the quarks or partons described by perturbation theory. Thus, some mechanism(s) should be implemented to transform the unobserved partons into the observed hadrons. These two energy scales are separated by a cutoff at Q_0, below which the partons are forced to convert into hadrons by some phenomenological model.

At the parton level, the jet evolution is described by parton branching. The probability of decay at each branching is based on summing all the ladder graphs in the leading-logarithmic approximation, neglecting the contribution from the interference of soft gluons. The effect of this approximation is that the mass squared of the partons in the jet cascade is strongly ordered.[3] The conventional Monte Carlo QCD branching is based on this fact. However, as the gluons become softer and softer, the contribution of crossed gluon graphs cannot be neglected as compared with the ladder diagrams. The soft-gluon branching out from a quark cannot see the color charge of the quark outside a certain cone along the original direction of the quark. With the inclusion of soft-gluon interference, the partons in the jet evolution are not only ordered in the mass squared, but also ordered in opening angles at successive branches.[4] The effect of soft-gluon interference has been implemented in a new Monte Carlo scheme by Marchesini and Webber to describe jet evolution.[2]

In the nonperturbative phase of the jet evolution, there are various models for converting the partons into hadrons: for example, the independent-fragmentation model, the string model, and the cluster phase-space model.[5] In the following analysis, we will employ Webber's Monte Carlo scheme and his version of the cluster phase-space model is used in hadronization. Since hadronization is still the least understood problem, we do not believe the cluster phase-space model is the ultimate answer. But because of its simplicity and its lack of some conceptual difficulties which appear in some other models (e.g., in Field-Feynman model, energy, color, and flavor are not conserved), it probably is a good method to explain many of the complexities in the hadronic final states.

The aim of our work is to investigate processes involved at and near heavy-quarkonium resonances. In fact, the study of two-jet events for e^+e^- annihilation has been carried out for several years and good agreement between experimental data and theoretical prediction is obtained.[1,2] Recently, more data at the on- and off-resonance region of upsilon decay have been accumulated.[6] It is possible to describe quarkonium decay by Monte Carlo QCD branching and in turn this will provide a more extensive test of the Monte Carlo scheme. Furthermore, it is very likely that the top quark and t-quarkonium will be discovered in the next generation of accelerators. Monte Carlo methods can also be applied to study some properties of t-quarkonium decay. The Monte Carlo model employed in our analysis is Webber's method, which includes as many QCD perturbative effects as possible and uses the cluster phase-space model as the hadronization scheme.

With all these in mind, the rest of the paper is organized as follows. In Sec. II the Monte Carlo cascade scheme with the inclusion of soft-gluon interference effects is reviewed briefly. In Sec. III we implement Webber's Monte Carlo scheme to describe jet formation both in decays of the upsilon and in nearby continuum states. In particular, we state some of the necessary modifications in Webber's original model in order to give a better agreement with data. Then, in Sec. IV, we extend the energy to the t-quarkonium region to look at some

interesting properties of the various decay modes of t-quarkonium. Finally, a short summary of our work is given in Sec. V.

II. MONTE CARLO METHOD

The Monte Carlo simulation of jets with soft-gluon interference effects is discussed fully in Ref. 2. The pictorial scheme of jet development is shown in Fig. 1. Basically, it consists of three phases: parton branching, cluster formation, and hadronization.

At the perturbative stage, the partons with large mass squared will decay into partons (always with smaller mass squared) with certain probability until they reach a cutoff value Q_0. The no-decay probability of an off-shell parton at q^2, when taking into account angle ordering, is given by the branching form factor:

$$\Delta(q^2)=\exp\left[-\int_{4Q_0^2}^{q^2}\frac{dk^2}{k^2}\times\int_{Q_0/k}^{1-Q_0/k}dz(P(z)\times\frac{\alpha_s[2z^2(1-z)^2k^2]}{2\pi}\right], \quad (1)$$

where

$$P(z)=\begin{cases}P_q^{qg}(z) & \text{for a quark leg,}\\ P_g^{gg}(z)+N_f P_g^{q\bar{q}}(z) & \text{for a gluon leg,}\end{cases}$$

and $P_q^{qg}(z)$, $P_g^{gg}(z)$, $P_g^{q\bar{p}}(z)$ are the Altarelli-Parisi splitting functions.[7] In this equation, we have used k^2 as the evolution variable; it is defined by $k^2=\omega^2\xi$, where ω and $\xi=q_1\cdot q_2/\omega_1\omega_2$ are the energy and angular variable of the parton, respectively. With this definition of the evolution variable, the angle ordering of the cascade has been taken into account. One peculiarity of the Webber-Marchesini model is to boost the system to a Lorentz frame such that the initial angular variable is smaller than 1. Then the light-cone momentum in restricted to the forward hemisphere and we can simply choose the parameter variable

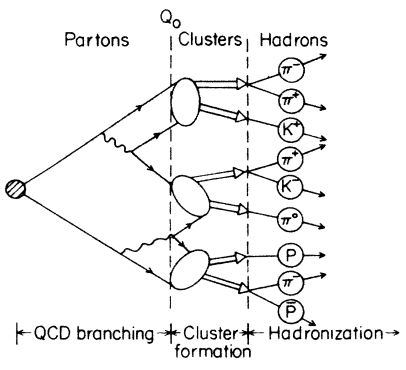

FIG. 1. Schematic picture of jet evolution.

in the Altarelli-Parisi splitting functions to be the energy of the partons. After the perturbative branching is terminated (i.e., all the partons reach the cutoff Q_0), the four-momenta of all the partons can be reconstructed.

In the preconfinement picture,[8] colorless clusters are viewed as the initial stage of hadron formation. In the original treatment, the colorless cluster is formed by a quark and an antiquark pair with all the gluons between them in the planar tree graph. However, this gives rise to phenomenological difficulties as the number of colorless clusters formed in this way is very small.[9] In the spirit of $1/N$ expansion, we recall that a gluon consists of two color lines while a quark or an antiquark consists of one color line. Thus, the gluons in the final stage of perturbative cascade can be forced to split into quark and antiquark pairs. The resultant quark and antiquark pairs in the overall final stage are grouped together to form colorless clusters as shown in Fig. 1. It should be noted that the colorless clusters prepared in this way are not the products of perturbation theory, but rather arise from an artificial way to make the concept of preconfinement useful phenomenologically.

In the process of hadron formation, the colorless clusters with known mass and quantum numbers are first allowed to decay into known resonances isotropically via a quasi-two-body decay mode. The resonances are prepared from the Particle Data Group tables.[10] The resonances used consist of the $0^-,1^\pm,2^+$ mesons and the $\frac{1}{2}^+,\frac{3}{2}^+$ baryons. The cluster decay is determined by the phase space available and the spin degeneracy of the chosen resonances. Because some of the colorless clusters have large mass, they are first split into smaller colorless clusters for isotropic decay to be reasonable.

In Webber's original model, there are three main parameters: the QCD scale Λ, the gluon-mass cutoff Q_0, and the maximum cluster mass M_f. The values for these three parameters are chosen to be

$$\Lambda=0.25\ \text{GeV},\quad Q_0=0.6\ \text{GeV},\quad M_f=3.5\ \text{GeV}. \quad (2)$$

To deal with different masses associated with quark flavors, different fission thresholds should be adopted for their associated clusters:

$$M_f(q)=[M_f{}^2+(m_q+m_{\bar{q}})^2]^{1/2}, \quad (3)$$

where m_q and $m_{\bar{q}}$ are the relevant constituent quark and antiquark masses. With these parameters, the Monte Carlo model gives satisfactory agreement with the data in e^+e^- annihilation over a wide range of energy.[2]

III. COMPARISON OF MONTE CARLO SIMULATION AND EXPERIMENTS AT THE UPSILON REGION

In recent years, much data have been obtained for upsilon decay and the continuum annihilation near the resonance.[6] It is thus interesting to use the QCD Monte Carlo model to simulate the processes at the upsilon region. For continuum annihilation, we just have the annihilation of e^+e^- into two quark jets. At the resonance, we expect the main decay mode is into three gluons. To implement

TABLE I. Multiplicities of various hadrons at 34 GeV (data taken from Ref. 11).

Hadron type	π^0	$\pi^{\pm}$	$K^{\pm}$	$K^0+\bar{K}^0$	$p+\bar{p}$	$\Lambda+\bar{\Lambda}$
Monte Carlo simulation	6.4	11.4	1.7	1.6	0.64	0.29
Experiments	6.1±2.0	10.3±0.4	2.0±0.2	1.6±0.1	0.8±0.1	0.28±0.04

this in the Monte Carlo model, the energies of the gluons are generated according to the matrix element

$$\frac{1}{\sigma}\frac{d^2\sigma}{dx_1dx_2}=\frac{1}{\pi^2-9}\left[\frac{(1-x_1)^2}{(x_2x_3)^2}+\frac{(1-x_2)^2}{(x_3x_1)^2}+\frac{(1-x_3)^2}{(x_1x_2)^2}\right], \tag{4}$$

where $x_1+x_2+x_3=2$ and $x_i=2E_i/Q$ are the energy fractions of the gluons. Then the evolution of these initial gluons is just the same as that in the two-jet case.

In Webber's model, the final gluons at the perturbative level are forced to split into up or down quarks and antiquarks for cluster formation. Strange quarks and antiquarks are not produced at this stage. This will mean that upsilon decay events have fewer kaons, because only a very small amount of strange quarks is generated by the perturbative branching of the three gluons. (In fact, there is about 0.1 primary strange quark produced per event in the two-jet case but no primary quarks in the three-gluon initial state.) Hence, if gluons are allowed to split only into up or down quarks and antiquarks in the nonperturbative prehadronization splitting, fewer strange particles are produced.

However, more kaons are observed experimentally in upsilon decay than in continuum annihilation. Therefore, we also allow the final gluons at the perturbative level to split into strange quarks and antiquarks. Thus there are two sources of strange-quark production at the nonperturbative stage. The first one is from final gluons splitting into quarks and antiquarks and the second is from cluster decay in which a quark-antiquark pair or a diquark-antiquark pair is generated to form two resonances.

As a consequence of the gluons splitting into strange quarks and antiquarks, a few modifications have to be made in Webber's program. First of all, the QCD cutoff Q_0 has to be increased so that the final gluons after QCD branching can split into strange quarks and antiquarks which produce clusters heavy enough to decay into two lightest strange hadrons. Second, allowing the final gluons to split into strange quarks and antiquarks inevitably produces more strange particles. Hence we simultaneously suppress the strange-quark production during cluster decay in order to maintain the successful aspects of the previous analysis.[2] In Webber's original model, the strange-quark weight and diquark weight during cluster decay are taken to be the same as the light-quark weight, but this must be changed.

In view of all these considerations, we choose the following parameters:

$$\Lambda=0.25\ \text{GeV},\quad Q_0=1\ \text{GeV},\quad M_f=3.5\ \text{GeV},$$
$$\text{strange-quark weight}=0.6\ , \tag{5}$$
$$\text{diquark weight}=0.8\ .$$

With this set of parameters, satisfactory results are obtained in the hadron multiplicities at 10 and 34 GeV (Tables I and II). It should be noted that more kaons are also generated at 34 GeV as compared with Ref. 2 and this gives better agreement with experimental results. The data used in our following comparison at the upsilon region are taken from Refs. 6 and 12.

In Fig. 2(a), we show the mass distribution of the light-quark colorless clusters for upsilon decay and nearby continuum annihilation. Note that in the case of upsilon decay, there are more high-mass clusters than in the case of continuum annihilation. This gives rise to the greater baryon production in upsilon decay than in continuum annihilation, as previously pointed out in Ref. 13. In fact, the high-mass clusters are mainly due to central clusters, which are defined as those clusters having each parton originating from different initial partons. In the configu-

TABLE II. Multiplicities of various hadrons at the upsilon region (data taken from Ref. 6).

	Hadron type	π^0	$\pi^{\pm}$	$K^{\pm}$	$K^0+\bar{K}^0$	$p+\bar{p}$	$\Lambda+\bar{\Lambda}$
Continuum annihilation	Monte Carlo simulation	3.9	7.0	1.11	1.05	0.36	0.15
	Experiments	3.0±0.7	8.3±0.4	1.3±0.2	0.92±0.12	0.40±0.06	0.066±0.010
Upsilon decay	Monte Carlo simulation	4.0	7.2	1.22	1.18	0.54	0.29
	Experiments	5.2±1.8	8.7±0.4	1.4±0.2	1.05±0.13	0.60±0.09	0.19±0.02

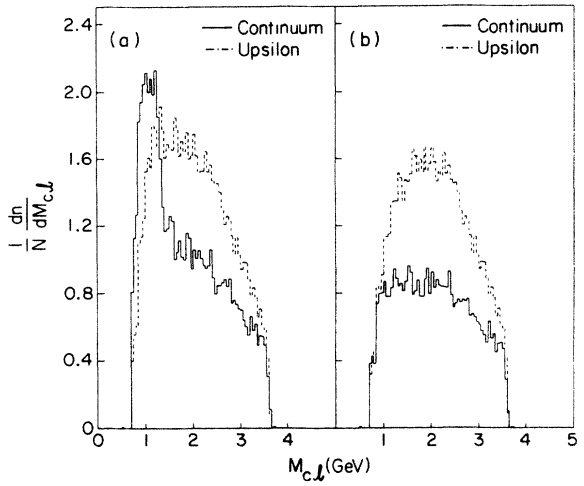

FIG. 2. Distributions of light-quark colorless cluster mass at upsilon region: (a) all clusters; (b) central clusters.

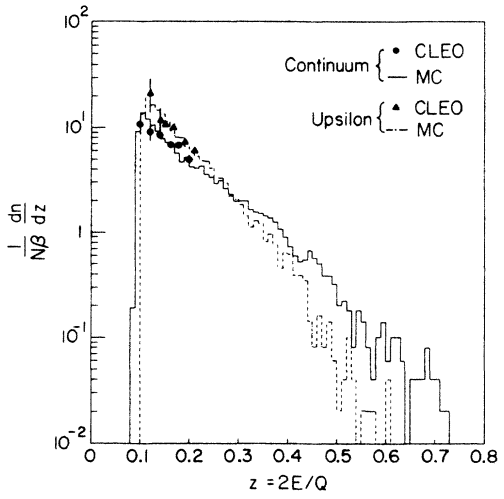

FIG. 4. Inclusive z spectra for $K^{\pm}$. Data from Ref. 6.

ration of upsilon decay into three gluons, there are more central clusters than in the continuum annihilation, as can be seen in Fig. 2(b).

Figures 3–5 show the single-particle inclusive spectra for charged pions, kaons, and protons as function of c.m. energy fraction $z=2E/Q$. In the literature, the data are always plotted as $(s/\beta)d\sigma/dz$ to reduce the energy dependence of the differential cross section. Since the cross section for upsilon spectra is not directly measurable because the beam energy resolution is wider than the resonance, it is more convenient to plot $(1/N)dn/dz$ instead of $(s/\beta)d\sigma/dz$, where N is the total number of events. In fact, the two plots are related by

$$\left[\frac{s}{\beta}\frac{d\sigma}{dz}\right]=\sigma s\left[\frac{1}{\beta N}\frac{dn}{dz}\right]. \tag{6}$$

The agreement between Monte Carlo simulation and data is generally satisfactory except in the case of the $\pi^{\pm}$ spectrum in the continuum annihilation measured by the CLEO group. CLEO detects more charged-pion multiplicity (8.3) than that from other experiments (e.g., compare a total charged multiplicity of about 7 detected by DASP). In Fig. 3, we also plot the $\pi^{\pm}$ data from Ref. 14. The Monte Carlo results are somewhat between the two sets of data.[15] Comparing upsilon decay with continuum annihilation, the particle spectra fall off more quickly with increasing energy in upsilon decay. This is anticipated since there are more particles in the final stage of upsilon decay and an individual hadron just carries less energy.

Figures 6–9 show the particle distribution for pions, charged kaons, and protons as functions of particle momentum fraction $x=2p/Q$. Again, there is a discrepancy between the Monte Carlo simulation and data in the $\pi^{\pm}$ spectra, especially at the small momentum re-

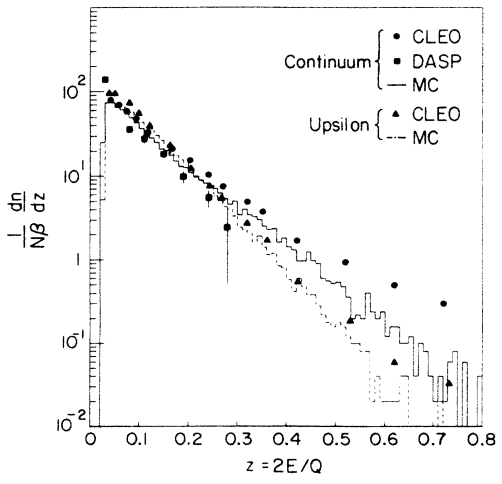

FIG. 3. Inclusive z spectra for $\pi^{\pm}$. Data from Refs. 6 and 14.

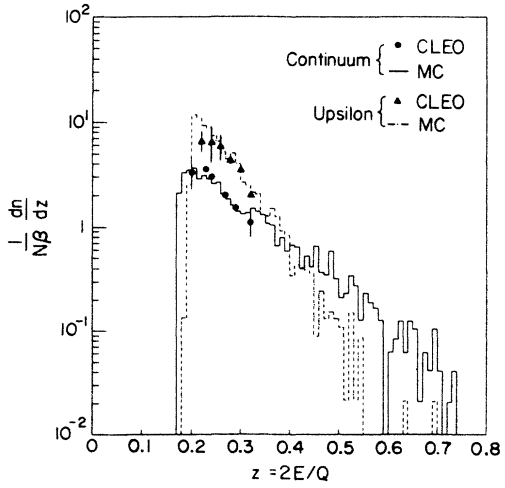

FIG. 5. Inclusive z spectra for $p+\bar{p}$. Data from Ref. 6.

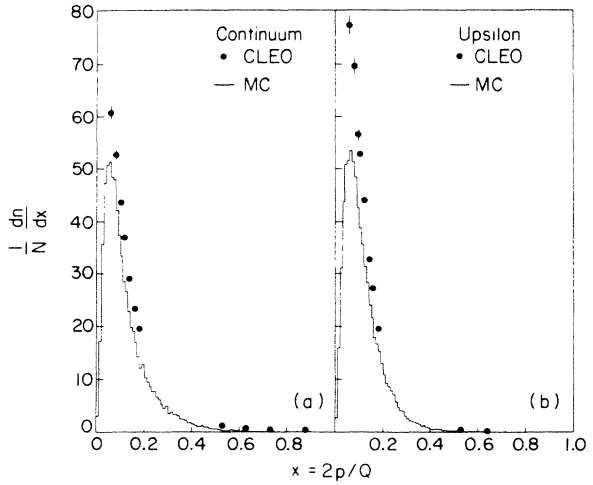

FIG. 6. Inclusive x spectra for $\pi^{\pm}$. Data from Ref. 6. (a) Continuum annihilation; (b) upsilon decay.

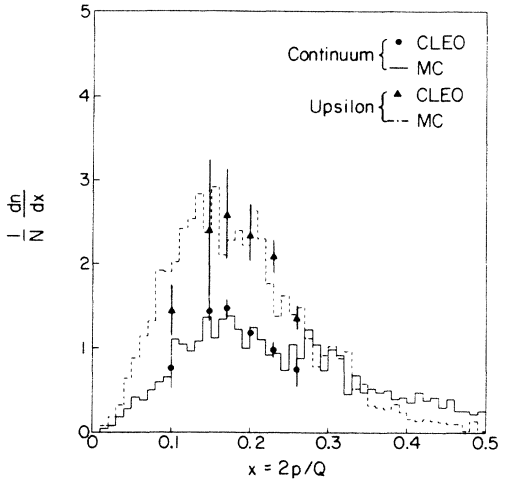

FIG. 8. Inclusive x spectra for $p+\bar{p}$. Data from Ref. 6.

gion. This is a reflection of the fact that the Monte Carlo method is unable to produce the large number of pions detected by CLEO. Of course, some of the parameters in the model can be adjusted to give better agreement. But then, many more pions will be generated at large energy (e.g., 34 GeV), which will cause a large discrepancy between data and Monte Carlo results at that energy. Further fine-tuning of the model has so far failed to completely reproduce the CLEO $\pi^{\pm}$ spectrum, and this is an area of further study. In Fig. 9 we also show the π^0 spectra. The agreement is good.

Figure 10 shows the charged-multiplicity fractions of pions, kaons, and protons as functions of particle momentum fraction. The agreement between Monte Carlo simulation and data is generally good. We clearly see that the proton multiplicity fraction is higher in upsilon decay than in continuum annihilation.

Figures 11—14 show the single-particle inclusive spectra for various kinds of heavier hadrons as functions of particle energy fraction. The agreement between Monte Carlo simulation and data is generally satisfactory except in the Λ spectrum in the continuum annihilation, in which the Monte Carlo simulation predicts more Λ particles than those observed experimentally. It should be noted that there is a larger discrepancy at high-energy fraction at the decay of upsilon; the Monte Carlo simulation gives many less particles at high-energy fraction of the particles. At 10 GeV, in order to maintain a fair amount of hadron multiplicity, the chance of a single particle to have high energy is very rare.

Figure 15 shows the rapidity distribution of all the charged hadrons. The Monte Carlo results are arbitrarily normalized since the data given in Ref. 6 are not corrected for acceptance and backgrounds, which cause the observed mean multiplicity to be about one to two units less than the true mean multiplicity. The Monte Carlo simu-

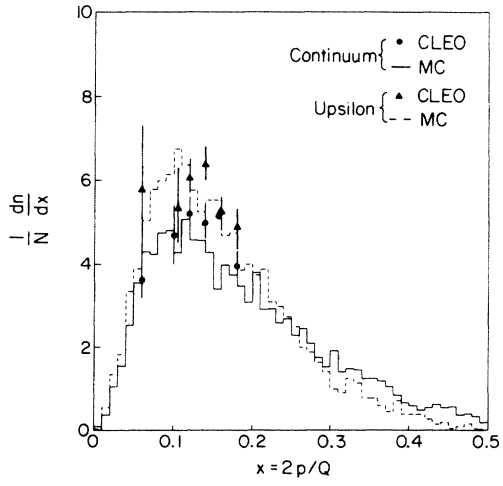

FIG. 7. Inclusive x spectra for $K^{\pm}$. Data from Ref. 6.

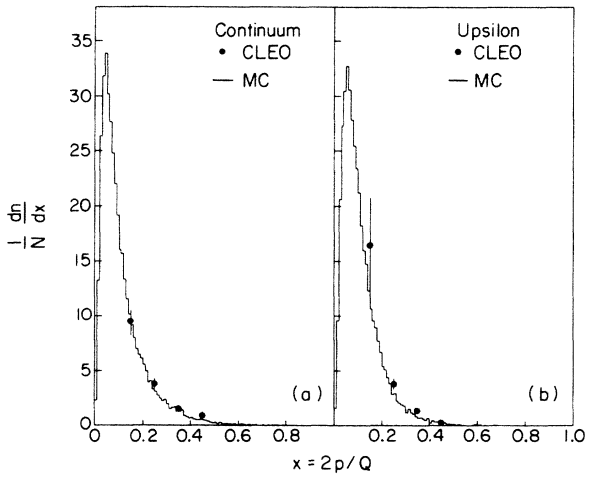

FIG. 9. Inclusive x spectra for π^0. Data from Ref. 6. (a) Continuum annihilation; (b) upsilon decay.

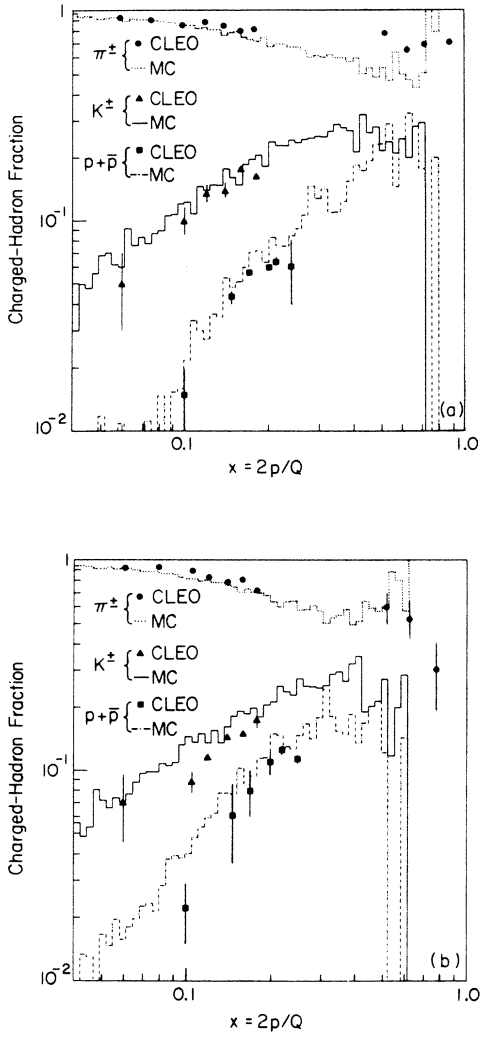

FIG. 10. Charged hadron fraction vs x. Data from Ref. 6. (a) Continuum annihilation; (b) upsilon decay.

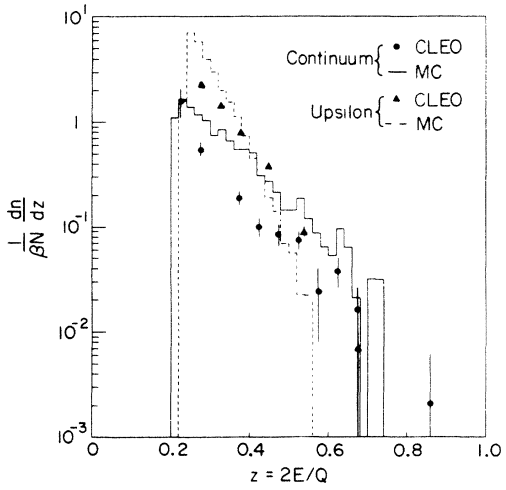

FIG. 12. Inclusive z spectra for $\Lambda+\bar{\Lambda}$. Data from Ref. 6.

lation gives similar shapes of the spectra in both upsilon decay and continuum annihilation. Again, the Monte Carlo simulation yields fewer particles at large rapidity. Finally, Fig. 16 shows the transverse-momentum-squared distribution of charged hadrons. The agreement between Monte Carlo results and data is satisfactory except the Monte Carlo simulation produces more hadrons with smaller transverse momentum squared in the spectra.

In conclusion, the Monte Carlo simulation generates satisfactory and consistent results for both upsilon decay and continuum annihilation near the resonance at 10 GeV. Of course, the most effective application of Monte Carlo QCD branching should be at high c.m. energy so that there is a large amount of phase space available for QCD branching before the partons reach the cutoff mass and nonperturbative effects can thus be reduced. Obviously, at 10 GeV, the phase space available for QCD branching is relatively small. In fact, in about 25% of the two-jet

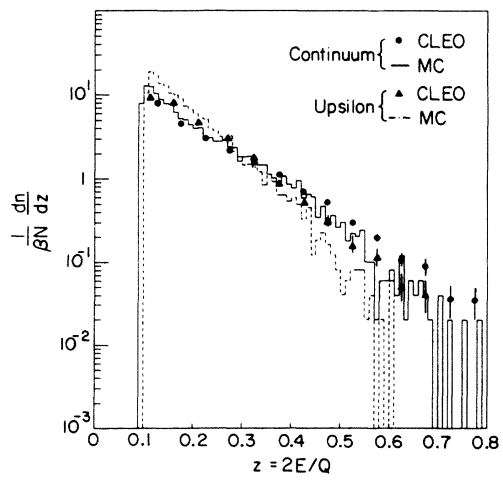

FIG. 11. Inclusive z spectra for $K^0+\bar{K}^0$. Data from Ref. 6.

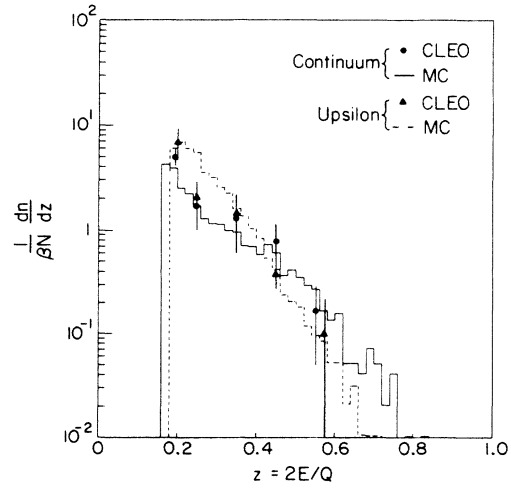

FIG. 13. Inclusive z spectra for $K^{*\pm}$. Data from Ref. 6.

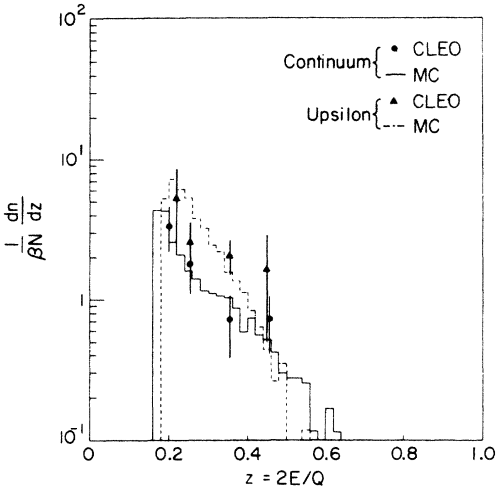

FIG. 14. Inclusive z spectra for $K^{*0}+\bar{K}^{*0}$. Data from Ref. 6.

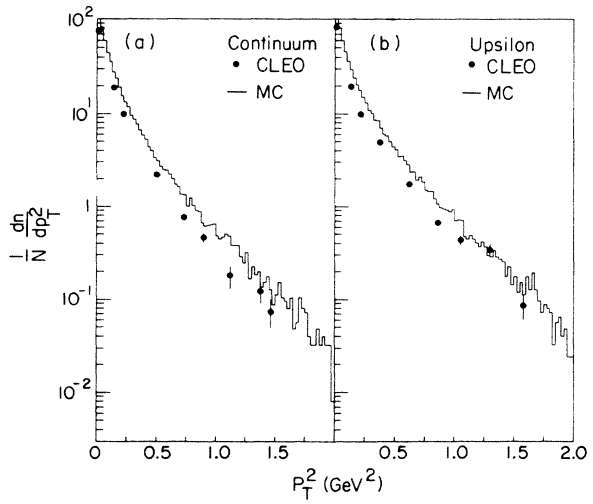

FIG. 16. Transverse-momentum-squared spectra for hadrons. Data from Ref. 12. (a) Continuum annihilation; (b) upsilon decay.

events the quark or antiquark does not emit a gluon via bremsstrahlung.[16] This means that the model converting the partons into hadrons has a large effect on the outcome of jet evolution. Perhaps this is the reason why we need more fine-tuning of the parameters. On the other hand, since jets are actually observed at this relatively small energy, it is instructive to apply the Monte Carlo simulation to investigate the situation. CLEO will obtain more data in the coming years. This will certainly provide us more information about the extent of applicability of the model.

IV. t-QUARKONIUM DECAYS

t-quarkonium has been an active area of research in the past few years. The experimental bound for the top quark is between 30 and 50 GeV.[17] If we take the top-quark mass to be 40 GeV, then the mass of t-quarkonium should be around 80 GeV. At this energy, the effect of the weak interaction cannot be neglected as compared with the strong interaction. The main decay modes of t-quarkonium are mainly (i) the annihilation decay into a fermion pair, (ii) annihilation into three gluons as in the case of upsilon decay, and (iii) single-quark decay.[18] These decay mechanisms are shown in Fig. 17. The relative importance of the various decay modes can be found in Ref. 18; we note that single-quark decay becomes more important when the mass of t-quarkonium increases. In fact, the decay rate of single quark decay exceeds that of annihilation decay into three gluons when the mass of t-quarkonium exceeds 50 GeV. Thus, this is an important decay mechanism at high energy. In the following, we use the Monte Carlo method to investigate the evolution of jets for t-quarkonium decays.

To implement the Monte Carlo method for the annihilation decays of t-quarkonium presents no difficulties. It is similar to upsilon decay and the continuum annihilation near this resonance as discussed in the last section. For single quark decay, either the top quark or antiquark decays weakly into a bottom quark and one quark-antiquark pair. (The decay into lepton pairs is neglected in our analysis since the quark pair gives richer structure in the final hadronic state.) The energy of the three quarks or antiquarks are generated according to the weak matrix element

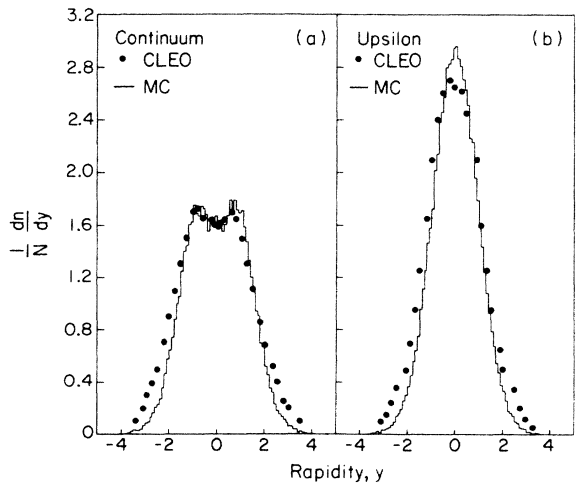

FIG. 15. Rapidity distribution of hadrons. Note that the Monte Carlo results are arbitrarily normalized to the data (see text). Data from Ref. 6. (a) Continuum annihilation; (b) upsilon decay.

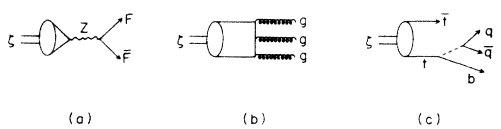

FIG. 17. Decay mechanisms of t-quarkonium: (a) annihilation into fermion pair; (b) annihilation into three gluons; (c) single-quark decay.

$$|\overline{M_{fi}}|^2 \propto (p_t \cdot p_i)(p_b \cdot p_j) , \quad (7)$$

where p_t, p_b, p_i, and p_j are the four-momenta of the top quark, bottom quark, and the other quark pair, respectively, and where we have neglected the effect of the charged-weak-boson propagator. These initial partons are then allowed to evolve as usual.

At the t-quarkonium energy, there should be an appreciable amount of bottom and charm hadrons produced in the jets. Since we currently lack much experimental information about the rich spectrum of these heavy hadrons, in order to investigate the various properties of these particles, the masses of the bottom hadrons are guessed. As in the light-quark hadron case, the bottom resonances used consist of the $0^-,1^\pm,2^+$ mesons and the $\frac{1}{2}^+,\frac{3}{2}^+$ baryons. The masses of the bottom mesons are taken from Ref. 19 while the masses of the bottom hadrons are evaluated from the following formula quoted from Ref. 20:

$$M_h = A + \sum_i \Delta m_i + B \sum_i \frac{\Delta m_i}{m_i} + C \sum_{i,j} \frac{1}{m_i m_j} + D \sum_{i,j} \left[\frac{1}{m_i^2} + \frac{1}{m_j^2} + \frac{16}{3} \frac{\mathbf{s}_i \cdot \mathbf{s}_j}{m_i m_j} \right] , \quad (8)$$

with

$$\Delta m_i = m_i - m_l ,$$

where m_l is the light-quark mass, m_i and $\mathbf{s}_i$ are the mass and spin of the quarks inside the hadron, and A,B,C,D are parameters. This choice of bottom resonances gives us a way to study the energy distribution of bottom mesons and baryons in the various decay modes of t-quarkonium. To investigate the lighter-hadron distributions, e.g., charm-hadron distribution, we need all the decay modes of the bottom resonances. However this is not known for most of the bottom resonances at present. Therefore, in investigating the charm-hadron spectra, the bottom quarks or antiquarks are forced to decay weakly into charm quarks or antiquarks at the end of the perturbative cascade.

Figure 18 shows the mass distribution of colorless clusters of light quarks of the two annihilation decay modes of t-quarkonium because they are similar to the decay

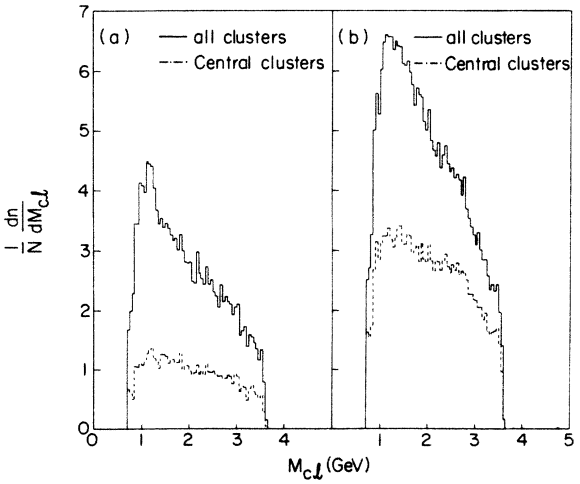

FIG. 18. Distributions of light-quark colorless cluster mass at t-quarkonium region: (a) annihilation into fermion pair; (b) annihilation into three gluons.

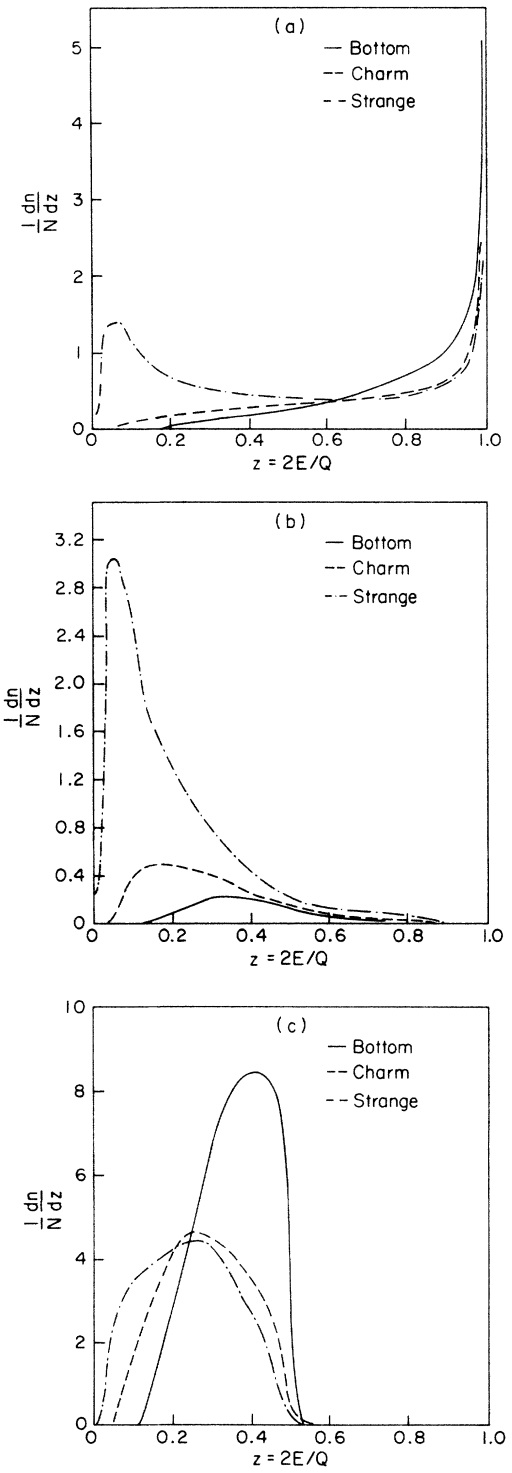

FIG. 19. Strange-, charm-, and bottom-quark distributions as functions of z: (a) annihilation into fermion pair; (b) annihilation into three gluons; (c) single-quark decay.

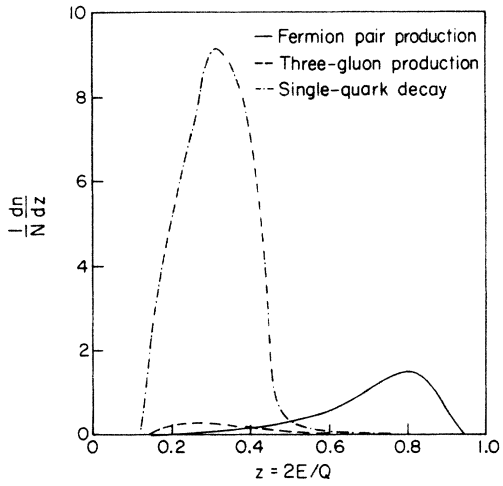

FIG. 20. Bottom-meson distributions as functions of z.

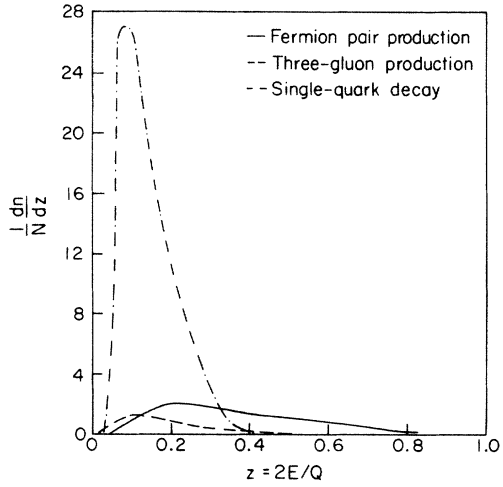

FIG. 22. Charm-meson distributions as functions of z.

mechanisms studied in the preceding section. Here at high energy, the importance of central clusters becomes less because the initial partons can always decay into some other partons by QCD branching. The light baryon contents of the two decay modes should be more similar in t-quarkonium decay than in the decays at 10 GeV. Of course, at this high energy, the effect of how the heavier hadrons (i.e., charm and bottom hadrons) decay into the lighter particles also influences the light-particle spectra. But still, the importance of the configuration of various decay mechanisms will be less than the situation in low c.m. energy.

Figure 19 shows the bottom-, charm-, and strange-quark distributions as functions of energy fraction of the quarks after the perturbative QCD branching stage. In the annihilation decay of t-quarkonium into two jets [Fig. 19(a)], the distributions of bottom and charm quarks peak more towards high energy while the strange quarks distribute more at small energy. This is because the heavy quarks are produced as primary partons and the cutoff mass for them is large so that the chances for them branching into other partons are relatively small. For strange quarks, apart from primary quark production, they can also be produced through gluons splitting perturbatively into quark and antiquark pairs.

In the annihilation decay of t-quarkonium into three gluons [Fig. 19(b)], there are no primary quarks. All the quarks and antiquarks come from gluon splitting. Of course it is more favorable for gluons to split into lighter quarks and antiquarks. Therefore we get more strange quarks than bottom and charm quarks. Furthermore, there is no enhancement in the distribution at high-energy fraction for the heavy quarks as this is a manifestation of primary quarks.

In single-quark decay [Fig. 19(c)], the situation is different. The top quark and antiquark in t-quarkonium can decay into a bottom quark and antiquark. Therefore we have a rich spectrum of bottom quarks at the perturbative stage. As shown in Fig. 19(c), these bottom quarks are concentrated at $z < 0.5$.

Figures 20–23 show the charm and bottom hadron distributions as functions of energy fraction of the hadrons. The spectra are plotted as $(1/N)dn/dz$ for each of the

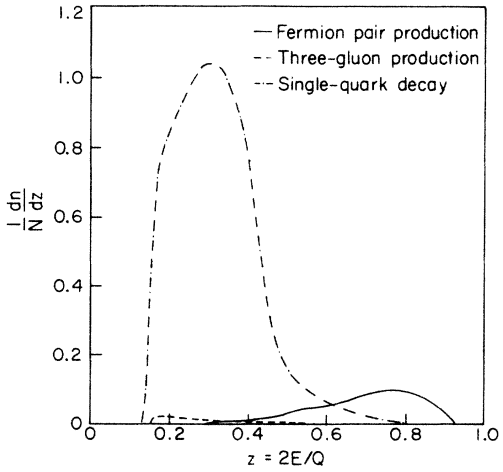

FIG. 21. Bottom-baryon distributions as functions of z.

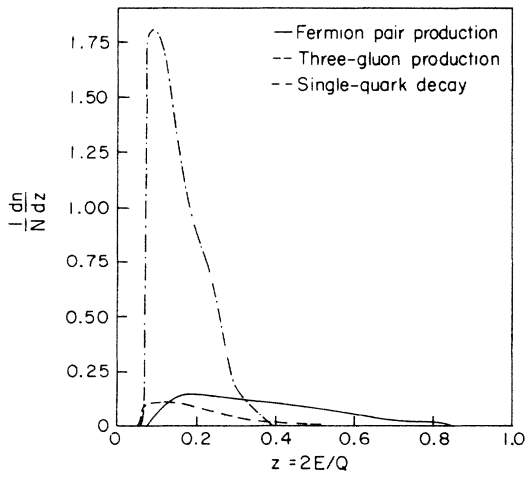

FIG. 23. Charm-baryon distributions as functions of z.

three decay modes of t-quarkonium. They actually represent the average multiplicity distributions of the various hadrons as functions of energy fractions. The spectra are reflections of the quark spectra discussed above. Again, it is noted that in single-quark decay, a large number of bottom hadrons are produced at relatively small energy fractions, while for the annihilation decays the amount of bottom hadrons is much smaller and they spread over a wider energy range. In the annihilation decay into three gluons, it is even more difficult to produce bottom hadrons because of the small amount of bottom quarks and antiquarks generated. We also note that because bottom baryons are usually about 0.5 to 1.0 GeV heavier than bottom mesons in our hadron mass spectrum, it is more favorable to form relatively lighter bottom mesons than bottom baryons from bottom clusters. If a greater amount of bottom baryons should be observed experimentally than predicted here, it must be due to nonperturbative effects, monitored by the stage determined by the cluster phase-space model.

V. CONCLUSION

We have applied Webber's model to investigate the evolution of jets for upsilon decay and continuum annihilation near this resonance in e^+e^- annihilation at around 10 GeV. Extensive comparison of various hadron spectra between Monte Carlo simulation and experiments has been carried out and satisfactory agreement is obtained. This is true in spite of the expectation that at this relatively low energy, nonperturbative effects will be more important and might limit the implementation of the QCD branching scheme.

We have also set the c.m. energy to 80 GeV (the postulated t-quarkonium mass) and investigated the various decay mechanisms of t-quarkonium. It turns out the heavy-quark and heavy-hadron spectra are quite different for the various decay modes. This might be of phenomenological interest in the future.

ACKNOWLEDGMENTS

It is a pleasure to thank Professor L. M. Jones for valuable discussions and continuous encouragement. I thank B. R. Webber for several discussions and sending us his new version of the Monte Carlo program. Discussions with P. Avery, S. Denham, and L. E. Holloway are also acknowledged. Thanks are also owed to the Illinois high-energy experimental group for use of their VAX computers. This work was supported by the U.S. Department of Energy under Contract No. DOEAC0276ER01195 Task P and by NATO collaborative Research Grant No. RG83/0779.

[1]R. Odorico, Nucl. Phys. **B172**, 157 (1980); G. Fox and S. Wolfram, *ibid.* **B168**, 285 (1980); T. Gottschalk, *ibid.* **B214**, 201 (1983).

[2]G. Marchesini and B. R. Webber, Nucl. Phys. **B238**, 1 (1984); B. R. Webber, *ibid*, **B238**, 492 (1984).

[3]For a review, see Yu. L. Dokshitzer, D. I. Dyakonov, and S. I. Troyan, Phys. Rep. **58**, 269 (1980).

[4]A. H. Mueller, Phys. Lett. **104B**, 161 (1981); A. Bassetto, M. Ciafaloni, G. Marchesini, and A. H. Mueller, Nucl. Phys. **B207**, 189 (1982); A. Bassetto, M. Ciafaloni, and G. Marchesini, Phys. Rep. 100, 201 (1984); B. I. Ermolaev and V. S. Fadin, Pis'ma Zh. Eksp. Teor. Fiz. 33, 285 (1981) [JETP Lett. 33, 269 (1981)]; Yu. L. Dokshitzer, V. S. Fadin, and V. A. Khoze, Phys. Lett. **115B**, 242 (1982); Z. Phys. C **15**, 325 (1983); **18**, 37 (1983); V. S. Fadin, Yad. Fiz. **37** 408 (1983) [Sov. J. Nucl. Phys. **37**, 245 (1983)].

[5]T. Gottschalk, lectures given at the 1983 Kupari-Dubrovnik Summer School, Yugoslavia, 1983 (unpublished); Caltech Report No. Calt-68-1075 (unpublished), and references therein.

[6]S. Behrends *et al.*, Phys. Rev. D **31**, 2161 (1985).

[7]G. Altarelli and G. Parisi, Nucl. Phys. **B128**, 298 (1977).

[8]D. Amati and G. Veneziano, Phys. Lett. **83B**, 87 1979).

[9]P. Mazzanti, R. Odorico, and V. Roberto, Nucl. Phys. **B193**, 541 (1981); Cho-Kuen Ng, Phys. Rev. D **31**, 469 (1985).

[10]Particle Data Group, Rev. Mod. Phys. **56**, S1 (1984).

[11]TASSO Collaboration, M. Althoff *et al.*, Z. Phys. C **17**, 5 (1983); TASSO Collaboration, R. Brandelik *et al.*, Phys. Lett. **108B**, 71 (1982); **94B**, 91 (1980); **105B**, 75 (1981).

[12]R. Cabenda, Ph.D. thesis, Cornell University, 1982.

[13]R. D. Field, Phys. Lett. **135B**, 203 (1984).

[14]H. Albrecht *et al.*, Phys. Lett. **102B**, 291 (1981).

[15]CLEO detects more charged pions than predicted, especially at large z. One might ask whether this indicates a problem with the theory, or an unsually high data set. We thus turn to comparison with other experiments, where the continuum two-jet cross section has been extensively studied. At 34 GeV, the agreement between TASSO and our Monte Carlo results is within 15% for, say, $z \geq 0.65$. Hence there is no serious problem with the calculations at large z.

[16]Using Webber's original set of parameters which contains a lower Q_0 value does not change this fact very much.

[17]UA1 Collaboration, G. Arnison *et al.*, Phys. Lett. **147B**, 493 (1984).

[18]J. H. Kühn and S. Ono, Z. Phys. C **21**, 395 (1984); **24**, 404(E) (1984); J. H. Kühn and K. H. Streng, Nucl. Phys. **B198**, 71 (1982); A. D. Martin, in *New Particles 1985,* proceedings of the Conference on New Particles, Madison, 1985, edited by V. Barger, D. Klein, and F. Halzen (World-Scientific, Singapore, in press).

[19]S. Godfrey and N. Isgur, Phys. Rev. D **32**, 189 (1985).

[20]A. De Rújula, Howard Georgi, and S. L. Glashow, Phys. Rev. D **12**, 147 (1975).